A Comparison of the Plastic-Flow Response of a Powder-Metallurgy Nickel-Base Superalloy Under Nominally-Isothermal and Transient-Heating Hot-Working Conditions

CrossMark

S.L. SEMIATIN, D.W. MAHAFFEY, D.J. TUNG, W. ZHANG, and O.N. SENKOV

The flow-stress behavior at hot-working temperatures and strain rates of the powder-metallurgy superalloy LSHR was determined under nominally-isothermal and transient-heating conditions. Two conventional methods, compression of right-circular cylinders and torsion of thin-walled tubes, were used for isothermal tests. A direct-resistance-heating technique utilizing torsion of round-bar specimens in a Gleeble® machine was applied for both isothermal and transient-heating conditions. When expressed in terms of effective stress and strain, baseline data determined by the two conventional methods showed good agreement. With the aid of a flow-localization analysis to assess the confounding influence of axial (and radial) temperature gradients on deformation uniformity, the flow stresses determined from nominally-isothermal Gleeble® torsion tests were shown to be broadly similar to those from the conventional tests. With regard to transient phenomena, Gleeble® tests were also useful in quantifying the effect of rapid heating and short soak time on the observed *higher* flow stress associated with a metastable microstructure. The present work also introduces two new test techniques using direct-resistance-heated torsion specimens. One involves *continuous* heating under *constant-torque* conditions, and the other comprises testing an individual specimen at a series of temperatures and strain rates. Using a single specimen, the former method enabled the determination of the apparent activation energy for plastic flow, which was similar to that determined from the series of isothermal tests; the latter provided a low-cost, high-throughput approach to quantify the flow behavior.

I. INTRODUCTION

DURING the last 40 years, the computer simulation of metal flow and microstructure evolution during metalworking operations has become a mature technology used widely in industry for selecting processing conditions, die and preform design, lubrication requirements, *etc*.[1–5] The application of such methods typically requires an extensive database of material properties, the description of friction and heat transfer phenomena at the workpiece-tooling interface, and the characteristics of the forming equipment itself. Key material characteristics include thermophysical properties (such as thermal conductivity/diffusivity and specific heat) and mechanical properties (such as the flow stress as function of strain, strain rate, temperature, and instantaneous microstructure/dislocation substructure).

A plethora of laboratory test techniques has been developed to gather flow-stress data. These include the simple compression, uniaxial-tension, and torsion tests.[6] For the simulation of hot-working processes at strain rates of the order of 0.1 to 100 s^{-1}, such tests are typically performed under nominally-isothermal conditions in which deviations from the initial test temperature arise primarily from deformation-induced heating that cannot be dissipated rapidly enough into the dies (as in compression tests) or sample shoulders (in tension and torsion tests) to maintain a uniform, constant temperature. These temperature increases can be taken into account when analyzing the flow response in an attempt to describe plastic-flow behavior that would pertain to an idealized, truly-isothermal condition. On the other hand, the neglect of such corrections can provide insight into the deformation resistance of material elements within very large workpieces (*e.g.*, billets, slabs, large open-die forgings) for which deformation heating gives rise to substantial temperature increases and concomitant changes in microstructure evolution.

Despite the utility of nominally-isothermal tests to characterize the flow behavior of metallic materials, many metalworking processes involve marked

S.L. SEMIATIN and D.W. MAHAFFEY are with the Air Force Research Laboratory, Materials and Manufacturing Directorate, AFRL/RXCM, Wright-Patterson Air Force Base, OH 45433. Contact e-mail: sheldon.semiatin@us.af.mil D.J. TUNG and W. ZHANG are with the Materials Science and Engineering Department, The Ohio State University, Columbus, OH 43210. O.N. SENKOV is with the Air Force Research Laboratory, Materials and Manufacturing Directorate, Wright-Patterson Air Force Base, and also with UES, Inc., 4401 Dayton-Xenia Road, Dayton, OH 45432.
Manuscript submitted September 21, 2016.
Article published online January 6, 2017.

temperature changes that greatly exceed those associated with deformation-heating alone. Examples include conventional hot forging and extrusion in which heat transfer between a hot workpiece and cold tooling (*i.e.*, so-called "die chill") can produce temperature drops of tens to hundreds of Kelvins per second in local regions near the interface. During such transients, a high-temperature, metastable microstructure may be retained to much lower temperatures that are experienced within the work material. In such cases, the instantaneous flow stress can differ substantially from that determined *via* a series of laboratory compression (or other) tests performed at various temperatures in which preheating enables the development of a near-equilibrium microstructure in terms of phase fractions, phase compositions, *etc*. In particular, the effect of die chill on flow stress and hence simulation predictions of forming loads can be very large for aerospace titanium and nickel-base alloys which exhibit large changes in phase fractions over a narrow temperature range.[7,8]

In contrast to conventional metalworking operations, marked *increases* in workpiece temperature concurrent with deformation characterize solid-state joining processes such as inertia- and linear- friction welding.[9,10] In these instances, friction generated by relative rotational or translational motion at the interface between two workpieces brings about rapid heating and eventual metal flow (upsetting) under the application of a force normal to the heated interface. For these processes, the rate of transient heating is typically of the order of several hundreds of Kelvins per second.

Attempts to understand plastic flow under transient conditions have focused primarily on so-called "on-cooling" and "on-heating" tests.[11] These techniques are usually based on the direct resistance heating of a tension or torsion specimen to a predetermined temperature, soaking at this temperature to equilibrate the microstructure, followed by rapid cooling or heating, respectively, to a specified test temperature at which deformation is imposed immediately (or after a short dwell time to achieve thermal equilibrium). The preponderance of such tests has sought to establish the effect of temperature path on ductility (*e.g.*, reduction in area), ultimate tensile strength, *etc*.[12–16] By contrast, recent work by Babu, *et al.*[17] has applied the technique to determine the transient flow response of a titanium alloy.

The work reported herein was part of a larger program on the description and simulation of inertia-friction welding (IFW) of dissimilar superalloys.[18–20] The overall goal of the present work was to develop a flow-stress database suitable for the finite-element-method (FEM) simulation of IFW. The specific objectives were fourfold: (1) establish and compare the high-temperature flow behavior of a typical powder-metallurgy nickel-base superalloy (LSHR) using nominally-isothermal methods including compression, thin-wall torsion, and torsion of round bars heated using a direct-resistance-heating method, (2) compare/contrast the measured isothermal flow behavior to similar measurements performed with an "on-heating" method, (3) develop and apply a method to determine flow stress under concurrent heating/ deformation conditions and interpret these results in the context of the isothermal measurements, and (4) develop/validate a rapid (high-throughput) method for determination of flow stress as a function of strain, strain rate, and temperature.

II. MATERIALS AND PROCEDURES

A. *Materials*

The nickel-base, powder-metallurgy (PM) $\gamma-\gamma'$ superalloy LSHR was used to establish the effect of test method on plastic-flow response under hot-working conditions representative of those developed during inertia-friction welding. LSHR (denoting "low-solvus, high refractory") was developed by NASA for jet-engine-disk applications. It provides an attractive balance of properties at the bore and rim of disks that have been subjected to a graded-microstructure heat treatment in which only the component rim is exposed above the γ'-precipitate solvus temperature to promote local growth of fcc γ grains.[21,22]

The program material was identical to that used in several previous investigations of the thermomechanical processing of PM superalloys.[23–25] It consisted of 230-mm-diameter extruded billet produced by Special Metals (Princeton, KY). Although the processing parameters for the billet were proprietary, extrusion of such materials is typically done at a temperature of ~1339 K (1066 °C) and a reduction/ram speed that imparts an effective strain rate of ~1 s^{-1}. The material composition is given in Table I; in the as-received condition, it had a fine, microduplex microstructure of γ grains and *primary* γ' precipitates, each of whose average diameter was ~2 μm, and ~0.33 volume percent of carbide/boride particles with an average diameter of 315 nm. The γ'-solvus temperature, T$_{\gamma'}$, was 1430 K (1157 °C). As determined by a series of long-time heat treatments followed by metallography, the alloy showed a typical variation of γ' volume fraction with temperature (Figure 1).[26] Microstructure evolution during preheating prior to mechanical testing is summarized in Reference 24.

B. *Experimental Procedures*

Three types of mechanical tests were performed to establish the plastic-flow response of the program material and to obtain input data for a parallel effort on the FEM simulation of inertia friction welding: (1) isothermal compression, (2) torsion of thin-wall cylinders, and (3) torsion of solid bars. For all experiments, test temperatures and strain rates were selected based on those typical of the hot deformation imparted during solid-state joining of superalloys.[18]

1. *Isothermal compression*
Isothermal, hot-compression data from a previous effort[24] were collected and served as part of the baseline to which results from other experiments were compared. For these measurements, cylindrical samples measuring 10-mm diameter × 15-mm height were extracted *via*

Table I. Chemical Composition (Weight Percentage) of LSHR Program Material

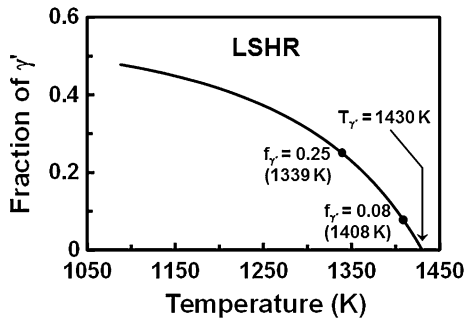| Co	Cr	Al	Ti	Mo	W	Nb	Ta	C	B	Zr	Ni
20.4	12.3	3.5	3.5	2.7	4.3	1.5	1.5	0.045	0.027	0.05	bal.

Fig. 1—Equilibrium solvus-approach curve for LSHR.[26]

wire EDM from the outer diameter of the extrusion (along the axial direction) and were coated with glass for lubrication. Following lubrication, the sample and silicon-nitride compression tooling (which were mounted in a 250 kN servo-hydraulic test system) were induction heated using an iron-chromium-aluminum alloy susceptor to a test temperature T of 1283 K, 1339 K, 1408 K, or 1450 K (1010 °C, 1066 °C, 1135 °C, or 1177 °C) in approximately 10 minutes. Following a soak at temperature for an additional 10 minutes, each sample was then compressed to an average axial (height) strain of 0.7. Constant true strain rates of 0.1, 1, and 10 s^{-1} were used. Following compression, the sample was lowered automatically and forced-air cooled.

Von Mises effective stress ($\bar{\sigma}$)—effective strain ($\bar{\varepsilon}$) curves were determined from average pressure (p_{av})—axial strain (ε) plots derived from the compression load-stroke data which were reduced assuming uniform deformation and corrected using a previously measured load-displacement (compliance) curve for the test-machine/load-cell system. The neglect of friction was estimated to lead to maximum errors in flow stress of the order of 3 pct for the sample geometry and height reduction used in the present work.[27]

2. Torsion of thin-wall cylinders

Additional baseline flow-stress data, which were complementary to the compression results, were obtained in a mode of simple shear *via* the torsion of tubular samples. Similar in design to that employed by various researchers in the 1980s,[28,29] the gage section comprised a short length L (3.18 mm), an outer radius r_s of 7.62 mm, and a wall thickness t of 0.88 mm. Torsion was performed in a custom-made, servo-hydraulic system which incorporated an indirect-resistance furnace with silicon-carbide heating elements. Each sample was preheated to test temperature in ~10 minutes, soaked for 10 minutes, and then twisted at a prescribed, constant rotation rate that produced a surface effective strain rate ($\dot{\bar{\varepsilon}}$) of 0.1, 1, 10, or 40 s^{-1}. The test

temperatures were 1283 K, 1339 K, 1408 K, and 1450 K (1010 °C, 1066 °C, 1135 °C, and 1177 °C).

Torque (M)—twist (θ) and rotation rate ($\dot{\theta}$) measurements from the torsion tests were converted to shear stress (τ)—shear strain (Γ), shear strain rate ($\dot{\Gamma}$), von Mises effective stress-effective strain, and von Mises effective strain rate ($\dot{\bar{\varepsilon}}$) using the following standard expressions[30]:

$$\bar{\varepsilon} = \Gamma/\sqrt{3} = r_s\theta/\sqrt{3}L \qquad [1]$$

$$\dot{\bar{\varepsilon}} = \dot{\Gamma}/\sqrt{3} = r_s\dot{\theta}/\sqrt{3}L \qquad [2]$$

$$\bar{\sigma} = \sqrt{3}\tau = \sqrt{3}M/(2\pi tr_s^2) \qquad [3]$$

3. Torsion of solid bars

Because of its ability to simulate a variety of thermomechanical processes, a Gleeble® 3800-499 thermal-mechanical test system (manufactured by Dynamic Systems, Inc. (DSI) Poestenkill, NY) was used to perform torsion tests under a variety of isothermal and transient-heating/deformation conditions. This system utilizes a servo-controlled hydraulic motor, a direct-resistance method of heating, and water-cooled stainless-steel grips. In addition, the equipment was outfitted with a slip ring that enabled the electric current to be left on and controlled during twisting. In all cases, round-bar samples with a standard DSI design (SMT001) were utilized and machined using standard lathe-turning and drilling operations; the geometry comprised a solid reduced section (measuring 20-mm length × 10 mm diameter), tubular shoulders (with an outer diameter of 14 mm and inner diameter of 8.33 mm), and a transition from tubular to solid over a short length just outside the reduced section. Except for tests in which failure occurred prematurely, a rotation of one revolution (corresponding to a surface effective strain of ~0.9) was applied.

For all experiments, testing was conducted in vacuum, and the sample temperature was controlled by a type-K thermocouple (with wire diameter of 0.25 mm) that was spot welded to the surface in the reduced section near the stationary end. Based on microstructure observations, the interior (bulk) temperature was estimated to be ~30 K (30 °C) *higher* than the measured surface temperature; except as noted, *such bulk values comprised the temperatures reported below*. To quantify axial temperature uniformity, a number of experiments were also performed with thermocouples welded at several additional locations along the reduced section.

Four types of Gleeble® torsion experiments were performed as follows

- Isothermal experiments, which were similar to the thin-wall torsion tests performed in the custom-made system with indirect-resistance heating. Test temperatures were 1316 K, 1339 K, 1389 K, and 1408 K (1043 °C, 1066 °C, 1113 °C, and 1135 °C). As for the thin-wall torsion tests, constant rotation rates that produced a *surface* effective strain rate of 0.1, 1, or ~10 s^{-1} were used.
- "On-heating" experiments comprising soaking for 10 minutes at a low temperature of 1144 K or 1339 K (871 °C or 1066 °C), heating to a higher test temperature of 1339 K or 1408 K (1066 °C or 1135 °C), respectively, in 3 seconds, soaking at this temperature for 10 to 20 seconds, and then twisting at a constant rotation rate to obtain a surface effective strain rate of 0.1 or 1 s^{-1}.
- Constant-torque/constant-heating-rate torsion tests. To determine the feasibility of determining plastic-flow behavior under transient-heating conditions with a limited number of samples, experiments consisting of the application of a nominally-constant torque (≈15, 30, or 60 Nm) at room temperature, heating at a constant rate of 10 or 40 K/s (10 or 40 °C/s), and the tracking of sample twist as the temperature increased were performed. Inasmuch as the DSI software did not enable torque as a control signal, the prescribed torques were obtained by adjusting the pressure of the oil delivered to the hydraulic motor. By this means, torque could be controlled to within approximately ±5 pct. of the desired value for a given experiment.
- Multi-temperature, multi-strain-rate torsion tests. To establish the feasibility of high-throughput determination of flow stress, several torsion tests consisting of preheating, soaking 10 minutes, and twisting at a series of 2 or 3 successively-higher temperatures [1339 K, 1366 K and 1408 K (1066 °C, 1093 °C and 1135 °C)] were conducted. At each temperature, 2 or 3 increments of rotation (corresponding to surface effective strain increments of ~0.15) were applied with a 5 minute dwell after each. Each increment was applied at a constant rotation rate that produced a surface effective strain rate of 0.01, 0.1, or 1 s^{-1}.

Because of the large number of experiments, only those tests that gave what appeared to be unusual results were duplicated.

As is usual practice, the torque-twist data from the Gleeble® torsion experiments were reduced to shear stress-shear strain values that corresponded to the outer surface of the reduced section. Despite the axial temperature and hence strain/strain rate variations that were developed in the Gleeble® torsion tests, *average* values of the strains and strain rates at the surface were determined using Eqs. [1] and [2]. The corresponding shear stress and effective stress at the outer radius r_s were estimated using the Fields-and-Backofen expression,[31] *i.e.*,

$$\bar{\sigma} = \sqrt{3}\tau = \sqrt{3}(3 + q^* + m^*)M/(2\pi r_s^3). \qquad [4]$$

In this relation, q* denotes the torque hardening exponent (determined from a plot of log M *vs* log θ), and m* is the rate-sensitivity of the toque (from a plot of log M *vs* log θ̇). At hot-working temperatures, the value of m* is comparable to that of the strain rate sensitivity of the flow stress, m. Because attention was focused on flow behavior at strains greater than the initial strain-hardening transient (*i.e.*, $\bar{\varepsilon} \geq 0.03$), q* typically had a value of approximately −0.1 to −0.2. With m* typically ≈0.25, the values of (3 + q* + m*) were thus ~3.1.

Despite the widespread use of the Fields-and-Backofen equation to determine the shear/effective stress during torsion of solid bars, it should be borne in mind that it is strictly applicable to deformation under *uniform-temperature* conditions. For strain rates of the order of 0.1 to 10 s^{-1}, however, non-negligible *radial* temperature gradients can be developed due to the variation of strain (and thus deformation heating) with position. Hence, the flow stresses deduced from the torque measured during torsion of solid bars might tend to be *higher* (in comparison with those from isothermal-compression tests and torsion of thin-wall tubes) because of the presence of metal near the center of the specimen whose temperature rise associated with deformation heating would be less than that near the outer regions of the specimen which experience larger strains. This effect would tend to be most noticeable for tests at lower temperatures and higher strain rates at which the flow stresses and the temperature dependence of the flow stress are highest. Furthermore, as will be discussed further below, the dependence of the instantaneous flow hardening/softening rate on strain in materials which undergo dynamic recrystallization may tend to lead to higher apparent peak stresses and broader flow-stress maxima than those observed in isothermal compression and thin-wall torsion tests.

C. *Modeling of Non-uniform Flow in Torsion*

As will be described below, the direct-resistance heating of solid bars in the Gleeble® system tended to produce an axial temperature gradient *ab initio*. To assess the influence of such gradients on the evolution of non-uniform flow and its effect on the prediction of flow stress, a flow-localization analysis similar to those described in References 32 and 33 was developed and applied.

The approach was based on the fact that the torque must be constant along the length of the sample to maintain equilibrium, *i.e.*, the axial variation of torque, δM, is equal to zero. Assuming that the strain, strain rate, and temperature gradients that evolve during torsion have negligible effect on the value of (3 + q* + m*), the torque equilibrium requirement (in conjunction with Eq. [4]) yields the expression $\delta\tau = 0$. The kinetics of flow localization during torsion are then readily quantified by discretizing the reduced section of

the torsion sample into a series of transverse slices, each with its own initial temperature, and mandating that each experience the same shear stress. For materials whose constitutive behavior follows the engineering flow law, viz.,

$$\tau = K_S(T)\dot{\Gamma}^m g(\Gamma) \qquad [5]$$

in which $K_S(T)$ denotes the temperature dependence of the shear stress and $g(\Gamma)$ describes the material strain-hardening/softening response, the instantaneous shear strain rates (and hence increments in shear strain) in each slice are determined as a function of the shear strain rate of a reference slice (taken to be the center slice in the present work). The application of the boundary condition specifying a constant overall twist rate then enables the determination of the shear strain rate for the reference slice and thus all of the slices. For each increment of time Δt, an increment of shear strain is then applied.

An upper bound on the degree of flow localization was established by assuming adiabatic conditions for which the temperature rise in each slice, ΔT, was calculated with the aid of the following equation[6]:

$$\Delta T = 0.95 \left(\tau \dot{\Gamma} / \rho C \right) \Delta t \qquad [6]$$

In Eq. [6], ρ, c denote the alloy density and specific heat, and it is assumed that 95 pct of the deformation work is converted into heat. For tests at high strain rates of the order of 1 s^{-1} or greater, the adiabatic assumption is a good approximation[27]; c was taken to be the average value over the temperature range of interest. However, because the shear strain rate varies radially across the section in torsion, an average value of the temperature rise was estimated based on the total work per unit volume applied to a solid-bar torsion sample. Taking $(3 + q^* + m^*)$ equal to 3.1, the pertinent expression can be derived with the use of Eqs. [2] and [4] is as follow:

$$\begin{aligned}
\text{Power/volume} &= M\dot{\theta}/(\pi r_s^2 L) \\
&= \left(2\pi r_s^3 \tau_S / 3.1\right)\left(L\dot{\Gamma}_S / r_s\right)/(\pi r_s^2 L) \qquad [7] \\
&= (2/3.1)(\tau_s \dot{\Gamma}_s)
\end{aligned}$$

The *average* temperature across the section of a solid-bar torsion sample is thus given by Eq. [6] in which τ and $\dot{\Gamma}$ are replaced by their values at the surface, and the prefactor is equal to $0.95 \times 2/3.1 = 0.61$.

III. RESULTS

The principal results from this investigation comprised the plastic-flow-observations for nominally isothermal compression/torsion tests and corresponding results from isothermal, "on-heating", continuous-heating, and multi-temperature Gleeble® torsion tests. These measurements are presented and discussed in the following sections.

A. Isothermal Compression/Thin-Wall Torsion Tests

Selected measurements of von Mises effective stress $\bar{\sigma}$ *vs* effective strain $\bar{\varepsilon}$ for LSHR from both isothermal compression tests and torsion of thin-wall specimens (Figure 2) revealed the expected dependence on temperature and strain rate. That is to say, the flow stress decreased with increasing temperature and decreasing strain rate. Moreover, for given combinations of temperature and strain rate, the $\bar{\sigma}$-$\bar{\varepsilon}$ curves exhibited relatively-good agreement for the two different modes of deformation. In all cases, the flow curves exhibited a peak stress at low strain ($\bar{\varepsilon} \sim 0.05$) followed by flow softening. The sources of the flow softening were twofold[24,25]: deformation heating and discontinuous dynamic recrystallization (DRX). The relative contributions of each are discussed in Section III-B.

B. Isothermal Gleeble® Torsion Tests

1. Flow curves

Compared to the behaviors observed from the hot compression and thin-wall torsion tests, the nominally-isothermal Gleeble® torsion tests yielded similar flow curves in terms of the broad temperature and strain-rate dependence of the flow stress and the occurrence of a peak stress at low strains followed by noticeable flow softening (Figure 3). A more quantitative assessment of the different types of measurements was obtained by comparing the flow stresses at two different levels of effective strain, *i.e.*, 0.05 (Table II) and 0.60 (Table III). At 1339 K (1066 °C), for example, the flow stresses at all strain rates were between 10 and 20 pct. higher for the Gleeble® torsion tests. These differences are further elucidated in Figure 4. Not only were the flow stresses higher, but the flow stress peaks were somewhat broader and shifted toward higher strains. At 1408 K (1135 °C), the flow-stress variation among the three deformation modes was only ~5 pct. or less for all strain rates and both strain levels.

Several sources of the difference in flow stress at lower temperatures [*e.g.*, 1339 K (1066 °C)] can be hypothesized:

(i) Axial temperature gradients. In the Gleeble® torsion tests, the direct-resistance-heating method led to an axial temperature variation of 10 K to 16 K (10 °C to 16 °C) from the (cooler) ends to the (hotter) center of the reduced section (for example, data in Figure 5). Thus, the *average* temperatures for these tests would have been 5 K to 8 K (5 °C to 8 °C) *higher* than the reported temperatures based on the control thermocouple located at the end of the reduced section. If the average temperature was higher, the flow stress from a Gleeble® test for a given nominal temperature should have been *lower*, not higher, than that from the hot compression/thin-wall torsion test at the same nominal temperature.

(ii) Temperature within the bulk cross section. The microstructure of samples heated in the Gleeble® suggested that the bulk temperature was
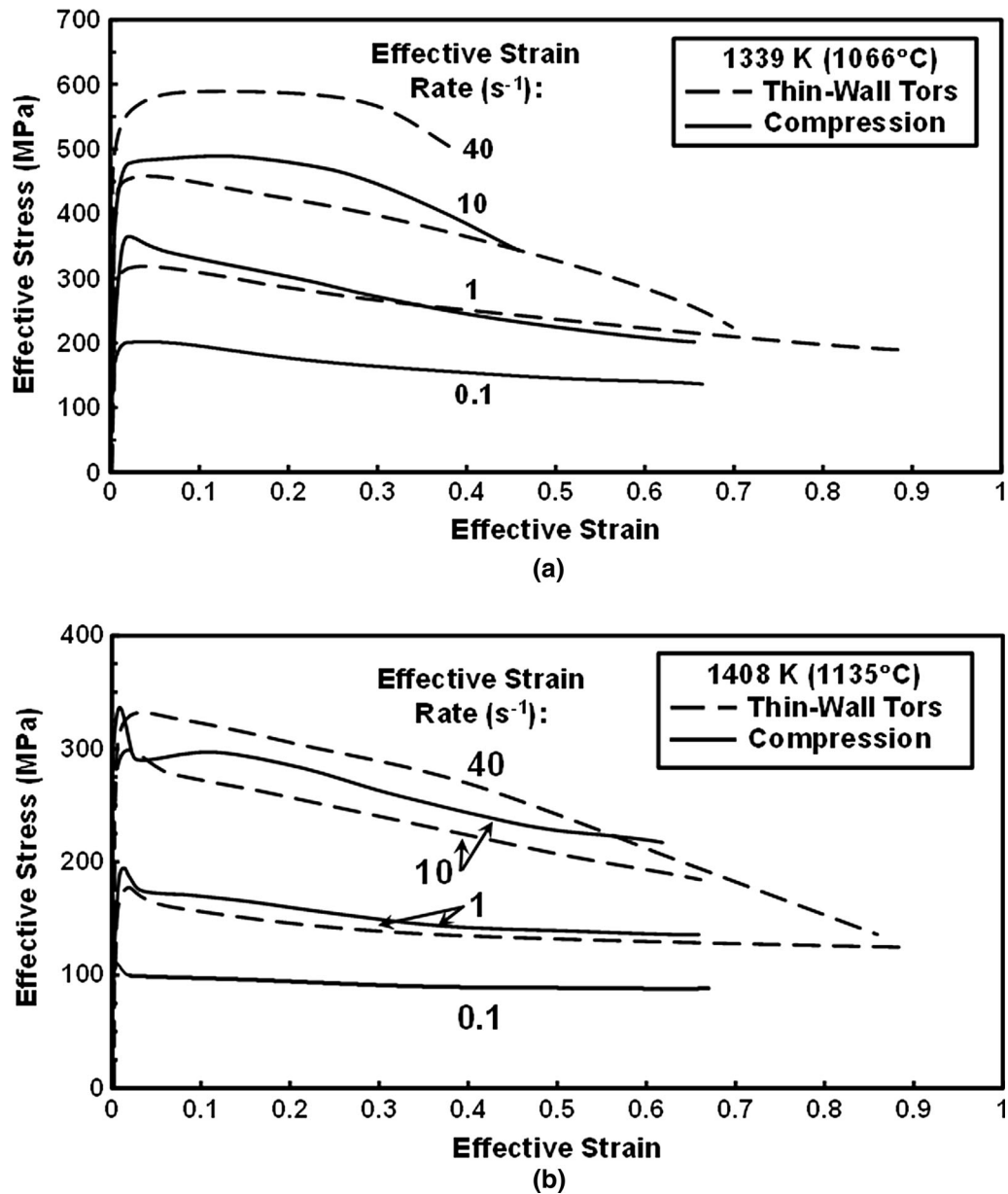
Fig. 2—Comparison of effective stress-effective strain curves for LSHR from isothermal, hot compression and thin-wall torsion tests performed at (*a*) 1339 K (1066 °C) and (*b*) 1408 K (1135 °C).

30 K (30 °C) hotter than that indicated by a thermocouple welded to the outer surface for temperatures of the order of 1300 K to 1400 K (1027 °C to 1127 °C). If this difference were only 20 K (20 °C), then the actual *average* test temperature for the samples deformed at nominally 1339 K (1066 °C) would have been lower by ~(30 − 20) − 6.5 = 3.5 K (3.5 °C). Such an amount also cannot explain the difference in flow stress.

(iii) Radial strain/temperature gradients and local flow-hardening/softening behavior. This is perhaps the most important factor. The flow hardening/softening response of materials which undergo DRX is a function of strain. At low strains (<5/6 of the strain corresponding

to the peak stress), strain hardening dominates relative to dynamic recovery, and the material exhibits flow *hardening*. At higher strains, the onset of dynamic recrystallization results in net flow softening. During the torsion of a solid bar of a material which undergoes DRX, therefore, the outer layers reach the peak stress first and begin to flow soften. However, the underlying layers whose strains are smaller ($\bar{\varepsilon} \sim r$) continue to flow *harden*. It may be possible that this continued hardening leads to an apparently-higher overall hardening rate and higher peak stresses in solid-bar torsion tests. An additional effect at high strain rates involves the tendency for radial temperature gradients to develop as a result of the radial stain gradient
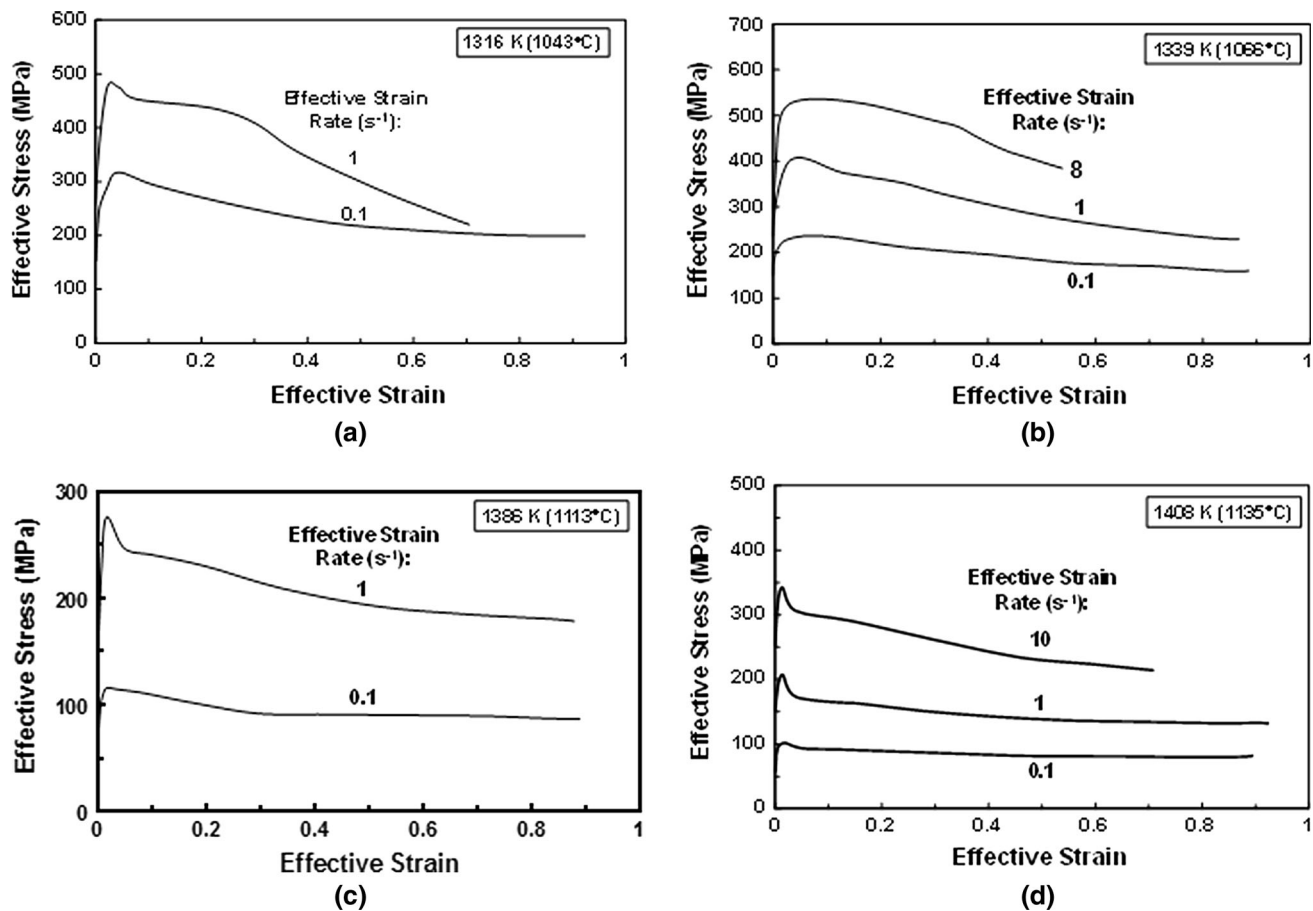
Fig. 3—Effective stress-effective strain curves for LSHR from nominally-isothermal Gleeble® torsion tests performed at (*a*) 1316 K (1043 °C), (*b*) 1339 K (1066 °C), (*c*) 1386 K (1113 °C), and (*d*) 1408 K (1135 °C).

Table II. Effective Stress (MPa) at an Effective Strain of 0.05

Test Type	T [K (°C)]	$\dot{\varepsilon} = 0.1\,\mathrm{s}^{-1}$	$\dot{\varepsilon} = 1\,\mathrm{s}^{-1}$	$\dot{\varepsilon} = 10\,\mathrm{s}^{-1}$
Gleeb Tors	1316 (1043)	307	465	—
Gleeb Tors	1339 (1066)	237	400	529
IsoComTors	1339 (1066)	201	329	467
Gleeb Tors	1386 (1113)	111	244	—
Gleeb Tors	1408 (1135)	97	169	301
IsoComTors	1408 (1135)	98	167	287

Table III. Effective Stress (MPa) at an Effective Strain of 0.60

Test Type	T [K (°C)]	$\dot{\varepsilon} = 0.1\,\mathrm{s}^{-1}$	$\dot{\varepsilon} = 1\,\mathrm{s}^{-1}$	$\dot{\varepsilon} = 10\,\mathrm{s}^{-1}$
Gleeb Tors	1316 (1043)	258	209	—
Gleeb Tors	1339 (1066)	171	261	357
IsoComTors	1339 (1066)	141	216	285
Gleeb Tors	1386 (1113)	91	187	—
Gleeb Tors	1408 (1135)	80	133	223
IsoComTors	1408 (1135)	87	132	207

and hence gradient in deformation-heating. Cooler metal in the interior could tend to lead to higher stresses than those generated during the torsion of thin-wall tubes. The complex, competing phenomena for torsion of solid bars (*i.e.*, radially-varying strain-hardening, dynamic recovery, and dynamic recrystallization in concert with an evolving temperature field) certainly merit consideration. However, such an analysis is beyond the scope of the current

work. Hence, the primary focus of the remainder of this paper concerns the broad trends of plastic flow for strains at and beyond the peak in the flow curves.

2. *Constitutive response*

One of the key inputs to the flow-localization simulations described in Section III-B-3 was the material constitutive response. To simplify the analysis, the initial flow-hardening portion of the flow curves was neglected, and the plastic-flow behavior of LSHR (in effective stress-strain terms) was described using a phenomenological relationship typical of those for deformation controlled by dislocation glide-climb at strain rates ≥ 0.1 s^{-1}, *viz.*,

$$\bar{\sigma}^n = K(T)\dot{\bar{\varepsilon}}h(\bar{\varepsilon}/\bar{\varepsilon}_p) = A\dot{\bar{\varepsilon}}\exp(Q/RT)\ h(\bar{\varepsilon}/\bar{\varepsilon}_p) \quad [8]$$

Here, n is the stress exponent of the strain rate ($=1/$m), A is a constant, Q is an apparent activation energy for plastic flow/dynamic recrystallization, R is the gas constant, $\bar{\varepsilon}_p$ is the effective strain corresponding to the peak flow stress (≈ 0.05), and $h(\bar{\varepsilon}/\bar{\varepsilon}_p)$ describes the flow-softening behavior. At $\bar{\varepsilon} = \bar{\varepsilon}_p$, h = 1, and $\bar{\sigma} = \bar{\sigma}_p$. Based on the data in Figures 2 and 3, plots of log $\bar{\sigma}_p$ *vs* log$\dot{\bar{\varepsilon}}$ indicated that m was between 0.2 and 0.3, or values typical of conventional hot working of metals.[34] Taking an average value for m = 0.25 for the sake of simplicity, n was thus equal to 4. Using data for $\dot{\bar{\varepsilon}} = 1$ s^{-1}, Q and A (Eq. [8]) were then determined from an Arrhenius plot of ln $\bar{\sigma}_p^4$ *vs* 1/T (Figure 6). (For the Gleeble® torsion data, T was taken to be the bulk temperature at the control-thermocouple location. An alternate plot with T being the approximate average temperature along the reduced section gave almost identical values of the material coefficients.) From Figure 6, Q/R was 71,140 Kelvins, thus yielding Q = 591 kJ/mol, and A(MPa^{4}s) = exp(-29.73).

The present value of apparent activation energy (Q) was somewhat higher than measurements for other superalloys (*i.e.*, 400 to 450 kJ/mol).[35,36] The difference is likely a result of variations in phase composition/phase fractions and a so-called mechanical effect that enters into the description of the deformation of two-phase alloys in general.[37] A perhaps more appropriate method of determining Q in which phase volume fractions do not change greatly with temperature is described in Section III-D.

For the deformation of nickel-base superalloys under conventional hot-working conditions, the strain dependence of the flow stress is typically controlled by DRX[24,25] which gives rise to flow softening for $\bar{\varepsilon} \geq \bar{\varepsilon}_p$. For the present work, the following phenomenological relation was used to fit the flow-softening response:

$$h = (\bar{\varepsilon}/\bar{\varepsilon}_p)^{q \cdot n} \quad [9]$$

in which the coefficient q was a negative number lying between -0.125 (lower temperatures in the test range) and -0.07 (higher temperatures in the test range).

3. *Flow-localization model results*

The key outputs of the flow-localization model comprised predictions of axial shear strain profiles and flow curves for torsion tests performed at an average surface effective strain rate of 1 s^{-1}. The initial axial temperature variation (δT) was taken to be 10 K or 16 K (10 °C or 16 °C), which mirrored measurements such as those shown in Figure 5. For simplicity, the temperature was assumed to increase linearly from the end of the reduced section (z = 0) to its mid-length (z = 10 mm) and to be symmetric about the mid-length to estimate the magnitude of the strain non-uniformity that does develop. The effect of flow softening due to
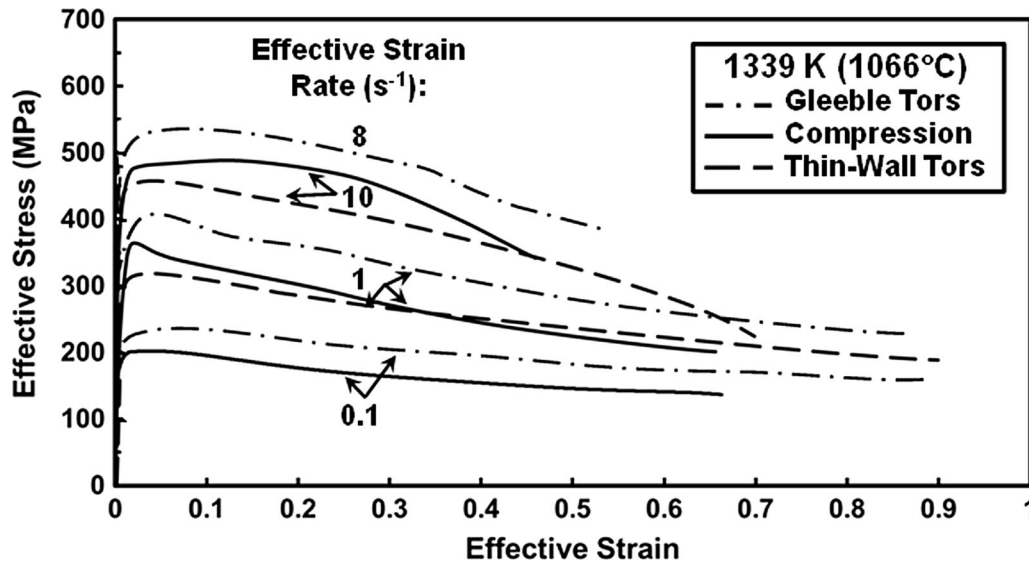

Fig. 4—Comparison of effective stress-effective strain curves for LSHR from isothermal, hot compression, thin-wall torsion, and Gleeble® torsion tests performed at 1339 K (1066 °C).
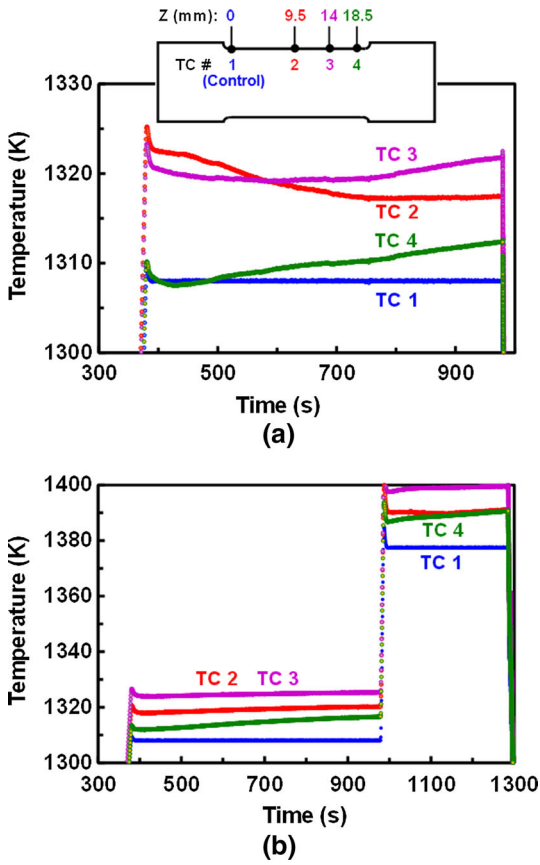
Fig. 5—Typical thermocouple measurements of the axial temperature variation at the surface of LSHR Gleeble® torsion specimens subjected to (a) soaking at a fixed temperature or (b) soaking followed by a rapid heating cycle.

Fig. 6—Arrhenius plot of peak-flow-stress data from isothermal-compression/thin-wall-torsion and Gleeble®-torsion tests at an effective strain rate of 1 s⁻¹.

Fig. 7—Comparison of measured values of local shear strain (data points) and flow-localization-simulation predictions assuming $\delta T = 10$ K (10 °C) (broken lines) or 16 K (16 °C) (solid lines) for Gleeble® torsion tests performed at a surface effective strain rate of 1 s⁻¹ and nominal test temperature of (a) 1316 K (1043 °C) or (b) 1386 K (1113 °C). In both figures, simulations incorporating deformation heating only are indicated by the red lines while those with both deformation heating and DRX-associated flow softening are indicated by the black lines.

DRX per se was highlighted using simulations in which the function $h(\bar{\varepsilon}/\bar{\varepsilon}_p)$ was not or was included in the input constitutive description.

From a qualitative perspective, model predictions of axial shear-strain profiles (Figure 7) showed a moderate dependence on the assumed magnitude of the initial temperature variation and the presence or absence of flow-softening in the constitutive model. Not surprisingly, the strain gradient developed at a specified level of rotation was predicted to be sharper for the larger value of δT. In a similar vein, inclusion of flow softening exacerbated the degree of localization as well. Model predictions of the shear-strain profile showed fair-to-good agreement with scribe-line measurements ($\Gamma = \tan\phi$, in which ϕ denotes the local angle between a scribe line, which was initially parallel to the torsion axis, and the axis after deformation). For a Gleeble® torsion test at 1316 K (1043 °C)/1 s⁻¹, for example, predictions incorporating DRX-associated flow softening agreed well with the measured shear strains except at the location at which the sample failed (Figure 7(a)). However, the simulation predictions tended to overestimate the shear strains at the ends of the reduced section. Such a difference was likely associated with the neglect of axial heat conduction into the shoulders which would strengthen material elements at the ends of
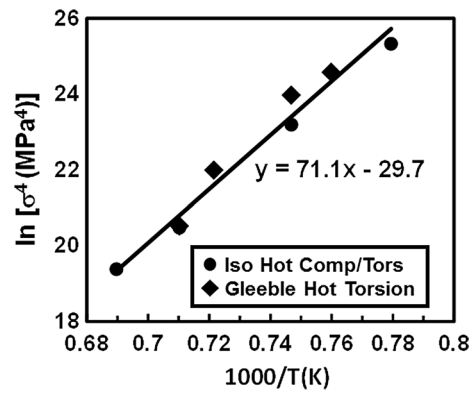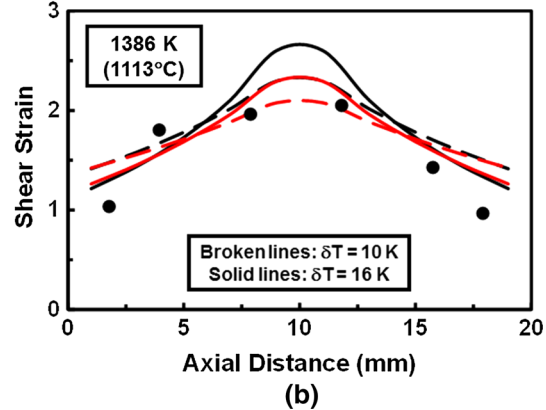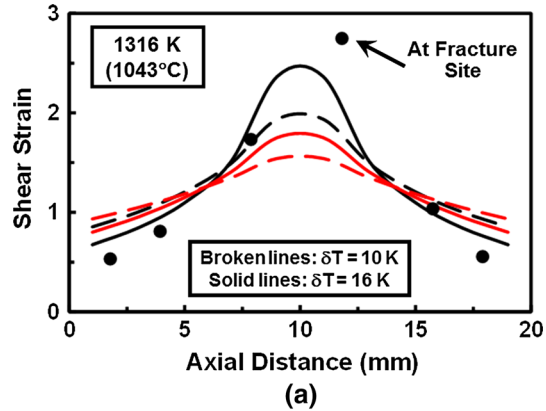
the reduced section and thus increase the strain gradient here. Similar agreement between predictions and measurements was obtained at 1386 K (1113 °C) (Figure 7(b)).

T [K (°C)]	Initial δT [K (°C)]	Without DRX		With DRX	
		$\bar{\varepsilon} = 0.6$	$\bar{\varepsilon} = 1$	$\bar{\varepsilon} = 0.6$	$\bar{\varepsilon} = 11$
1316 (1043)	10 (10)	0.154	0.241	0.389	—
1316 (1043)	16 (16)	0.155	0.246	0.400	—
1339 (1066)	10 (10)	0.123	0.195	0.363	0.461
1339 (1066)	16 (16)	0.122	0.197	0.361	0.468
1386 (1113)	10 (10)	0.069	0.113	0.219	0.283
1386 (1113)	16 (16)	0.068	0.112	0.220	0.285
1408 (1135)	10 (10)	0.056	0.092	0.197	0.254
1408 (1135)	16 (16)	0.055	0.091	0.198	0.255

Table V.   Measured Values of Flow-Softening Index (F) for $\dot{\bar{\varepsilon}} = 1\,s^{-1}$

Test Type	T [K (°C)]	$\bar{\varepsilon} = 0.6$	$\bar{\varepsilon} = 1$
Gleeb Tors	1316 (1043)	0.551	—
Gleeb Tors	1339 (1066)	0.348	0.464
IsoComTors	1339 (1066)	0.343	0.454
Gleeb Tors	1386 (1113)	0.234	0.299
Gleeb Tors	1408 (1135)	0.213	0.252
IsoComTors	1408 (1135)	0.210	0.278

The flow-localization model was also helpful in establishing the relative contributions to measured flow-softening levels in isothermal compression/ thin-wall torsion experiments and Gleeble® torsion tests (Tables IV, V; Figure 8). Specifically, the levels of flow softening at average surface effective strains of $\bar{\varepsilon} = 0.60$ and $\bar{\varepsilon} = 1$ were quantified using the index, F:

$$F = (\bar{\sigma}_p - \bar{\sigma})/\bar{\sigma}_p \qquad [10]$$

Simulation predictions for a given test temperature (Table IV) indicated that the level of the initial temperature variation (δT) in Gleeble® torsion tests had essentially *no* effect on the value of F at a given strain level. Furthermore, a comparison of the values of F for the cases with and without microstructure-related (DRX) flow softening (*i.e.*, the function h in Eqs. [8] and [9]) indicated that approximately 60 to 70 pct. of the overall decrease in stress was due to this source and 30 to 40 pct. was associated with deformation (adiabatic) heating.

Experimental measurements (Table V) showed that F was essentially identical for the isothermal compression/ thin-wall torsion tests and the Gleeble® torsion tests performed at comparable temperatures. In addition, the predicted values of F for cases including microstructure-related softening (Table IV) showed excellent agreement with the measurements (Table V) except for T = 1316 K (1043 °C). The difference at this temperature may be related to the occurrence of fracture at $\bar{\varepsilon} \sim 0.6$, whose effect on plastic flow was not captured in the flow-localization analysis.

The flow-localization simulations also highlighted possible differences in stress-strain response associated with the assumption of uniform shear strain along the axis when reducing Gleeble® M−θ data. For this purpose, simulated effective stress-strain curves for an initial axial temperature variation of δT = 16 K (16 °C), with and without microstructure-based softening, were compared to parallel predictions for cases involving δT = 0 K (0 °C) but different initial temperatures equal to the minimum, average, or maximum temperature in the former case (Figure 8). Moreover, in all instances, the effective stress was plotted as a function of the surface effective strain based on the length of the reduced section and the overall twist. Despite the development of axial strain and strain rate gradients in simulations with an initial δT = 16 K (16 °C), a comparison of the flow curves for such cases were almost identical to those from the corresponding simulations for which the initial (uniform) temperature was equal to the *average* of the non-uniform case (Figure 8). Simulations taken to effective strains greater than unity (not shown), however, did indicate an increasing divergence in the curves as the flow behavior for samples with the initial temperature gradient became less "quasi-stable" in nature. Hence, for plastic-flow behaviors such as those described herein, the axial strain and strain rate non-uniformity that evolved as a result of the initial temperature gradient could be largely neglected in reducing torque-twist data to determine effective stress-strain behavior at least for effective strains of 1 or less.

C. *On-Heating Gleeble® Torsion Tests*

The flow response of Gleeble® torsion samples tested on-heating showed some similarities and some differences relative to nominally-isothermal tests depending on specific test temperature and strain rate (Figure 9). For instance, the flow curves of samples pre-heated/soaked at 1144 K (871 °C), rapidly heated to 1339 K (1066 °C), and held 20 seconds before torsion were very similar to the corresponding results for specimens preheated and soaked 10 minutes prior to torsion at 1339 K (1066 °C) (Figure 9(a)); the only noticeable difference was the occurrence of a small amount of torque-cell "ringing" for the higher-strain rate on-heating experiment. These observations suggested that the microstructures developed prior to twisting were nearly the same in both sets of experiments. The similarity of the "on-heating"
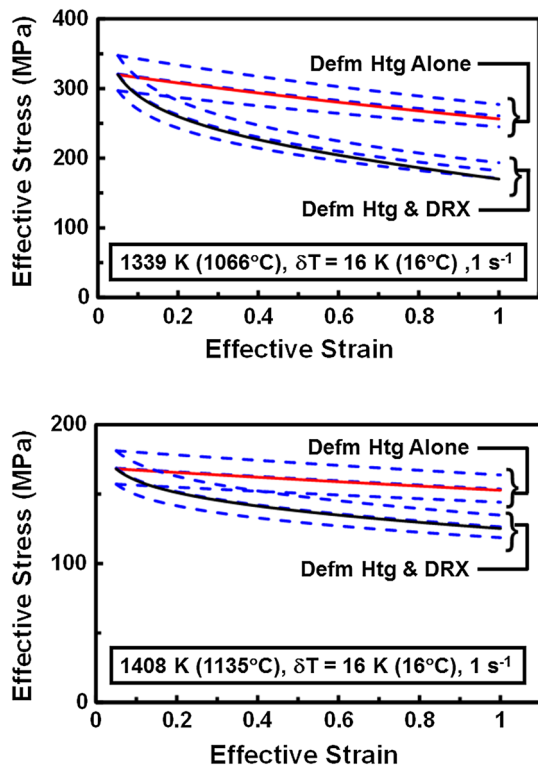
Fig. 8—Flow-localization model predictions of effective stress-average effective strain curves (solid lines) for the torsion of round bar samples with an initial δT of 16 K (16 °C) using an input constitutive response with or without DRX. The results are compared to simulations for samples with a uniform initial temperature equal to the maximum (upper broken line), average (middle broken line), or minimum (lower broken line) in the corresponding non-uniform-temperature simulation.

Fig. 9—Comparison of flow curves from isothermal and on-heating ("non-equilibrium") Gleeble® torsion tests performed at surface effective strain rates of 0.1 and 1 s^{-1} and test temperatures of (a) 1339 K (1066 °C) or (b) 1408 K (1135 °C). The preheat temperatures for the on-heating tests are indicated in the figures.

microstructure to that developed during soaking at 1339 K (1066 °C) can be rationalized on the basis of the fact that the original billet from which all specimens had been extracted was likely extruded near this same temperature. Thus, the γ grain size and primary γ' size and volume fraction had largely been established prior to testing. Secondly, the size (~300 nm) of cooling γ' formed after extrusion was likely fine enough to dissolve rapidly during the heat-up and short soak imposed for the on-heating specimens.

Flow-curve comparisons for on-heating [from T = 1339 K (1066 °C) → 1408 K (1135 °C)] and isothermal tests at 1408 K (1135 °C) revealed a more complex behavior (Figure 9(b)). In particular, the flow curves for the two types of tests at an effective strain rate of 0.1 s^{-1} were almost identical. The somewhat higher flow stress for the on-heating test at this strain rate can be rationalized on the basis of a retention of a higher-than-equilibrium volume fraction of primary γ' and concomitant finer γ grain size during deformation compared to the isothermal test involving a long presoak time prior to deformation (Figures 10(a) and (b)). With regard to the precipitate effect, the equilibrium volume fractions of γ' at 1339 K and 1408 K (1066 °C and 1135 °C) are 0.25 and 0.08, respectively
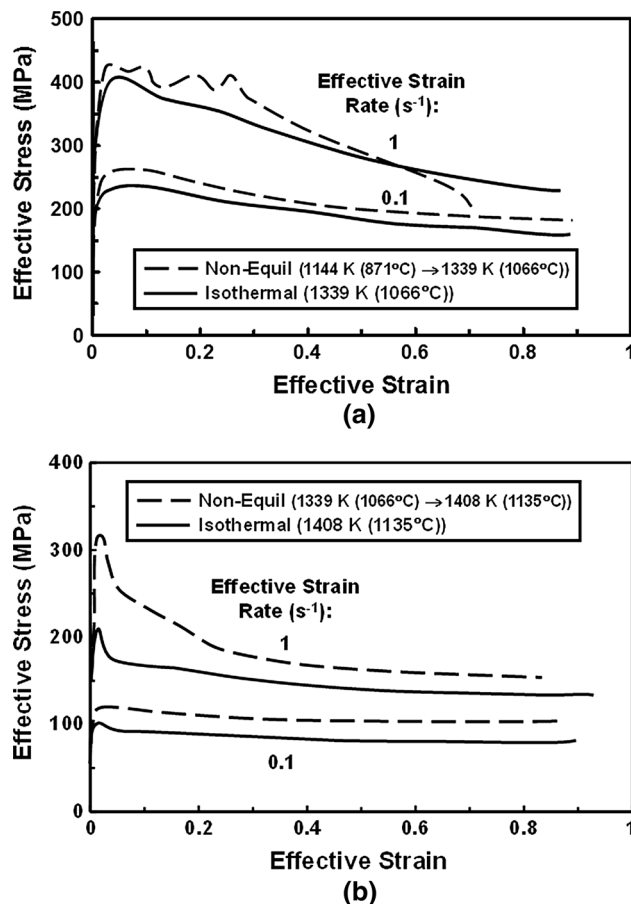
(Figure 1). As the micrograph in Figure 10(b) indicates, the on-heating sample at the end of deformation still contained 0.16 volume fraction of γ', which is less than the amount at its lower (preheat) temperature of 1339 K (1066 °C) (i.e., 0.25), but still greater than 0.08.

The Gleeble® torsion flow-stress results at 1 s^{-1} revealed a much larger difference (Figure 9(b)). Differences in the same two microstructural features (Figures 10(c) and (d)) (as well as possibly retained dislocation substructure) coupled with the very short duration of deformation at the higher strain rate can be used to rationalize the contrasting flow behaviors. On-heating-soak time at the deformation temperature was also concluded to be an important factor with regard to the retention of a non-equilibrium microstructure (and possibly substructure). This effect was quantified by comparing flow curves for on-heating tests involving either a 10 or 20 seconds soak time upon reaching the test temperature (Figure 11).

The comparison of isothermal and on-heating tests also revealed the beneficial effect of retaining a fine γ grain size on retarding cavitation. This effect is illustrated in Figure 10 in which high stress levels generated
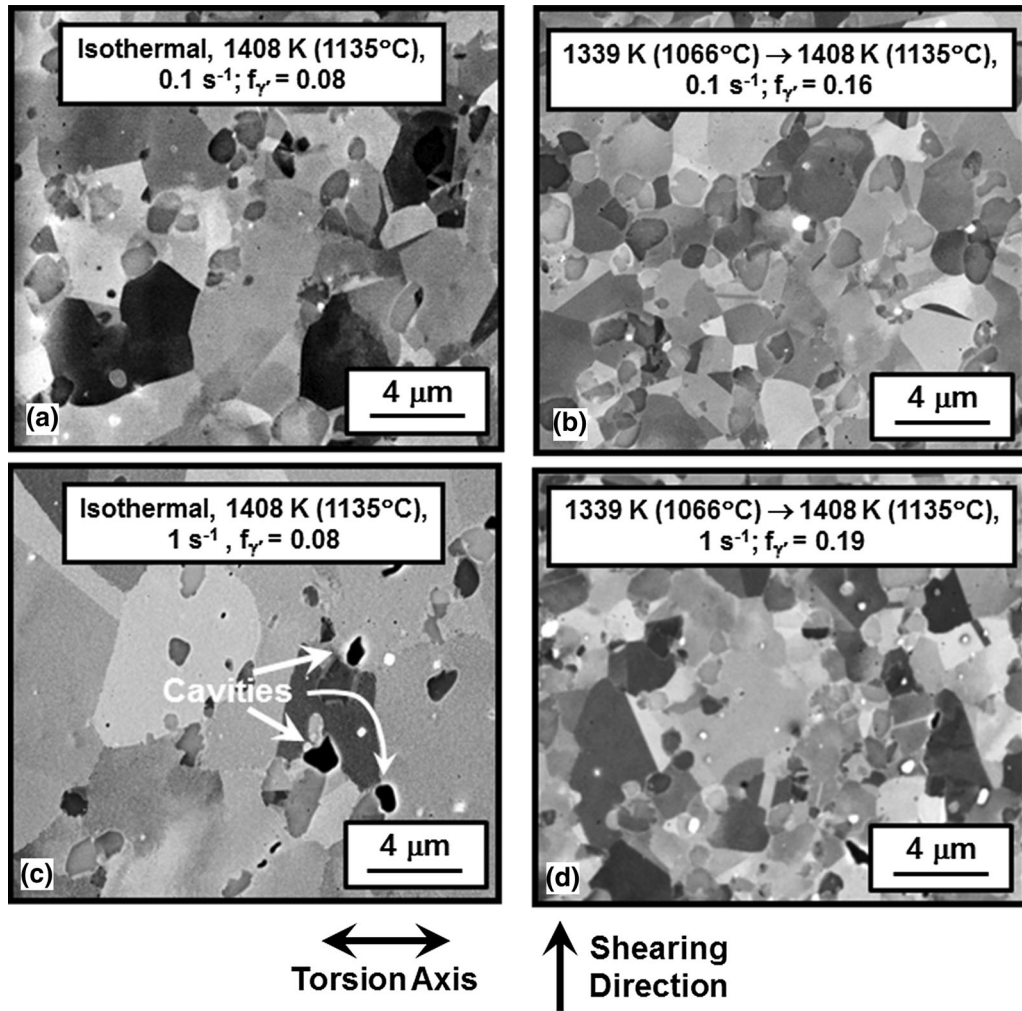
Fig. 10—Backscatter electron images of the microstructures developed at the outer diameter of (*a, c*) isothermal or (*b, d*) on-heating Gleeble® torsion tests performed at 1408 K (1135 °C) and an average surface effective strain rate of (a, b) 0.1 s^{-1} or (c, d) 1 s^{-1}.

at 1 s^{-1} and a γ grain size which had coarsened during preheating led to noticeable cavitation in the *isothermal* sample tested at 1408 K (1135 °C) (Figure 10(c)). By contrast, the smaller γ grain size retained in the corresponding on-heating sample (Figure 10(d)) exhibited only a few, small cavities despite its high flow stress.

D. *Constant-Torque, Continuous-Heating Gleeble® Torsion Tests*

Nominally-constant-torque tests performed under continuous (constant-rate) heating conditions provided insight into the effect of transient conditions (such as may be experienced during solid-state joining) on plastic-flow behavior. For example, twist measurements for various combinations of applied torque and heating rate (dT/dt) (Figure 12(a)) exhibited the expected increase in twisting *rate* [dθ/dt = (dθ/dT) × (dT/dt)] as the temperature increased during each experiment. From a qualitative standpoint, the twist rate/strain rate in each experiment began at a rather low value at low temperature and increased rapidly as the material began to soften with increasing temperature. A comparison of
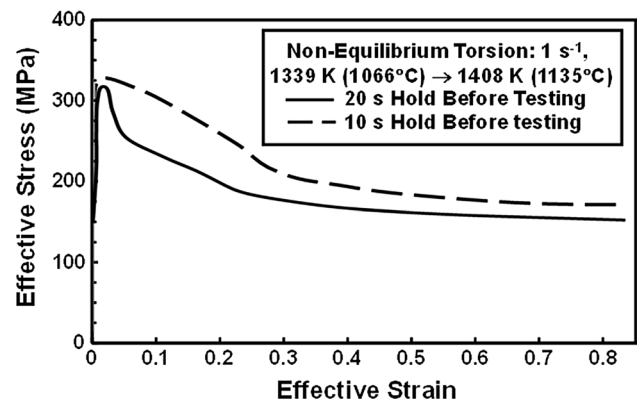

Fig. 11—Comparison of flow curves from on-heating Gleeble® torsion tests [(1339 K (1066 °C) → 1408 K (1135 °C)] for which the soak time at test temperature prior to twisting was either 10 or 20 s.

two data sets for a torque of ~60 Nm (Figure 12(a)) revealed a limited effect of heating rate on deformation response per se at least for rates between 10 and 40 K/s (10 and 40 °C/s). Not surprisingly, the temperature at
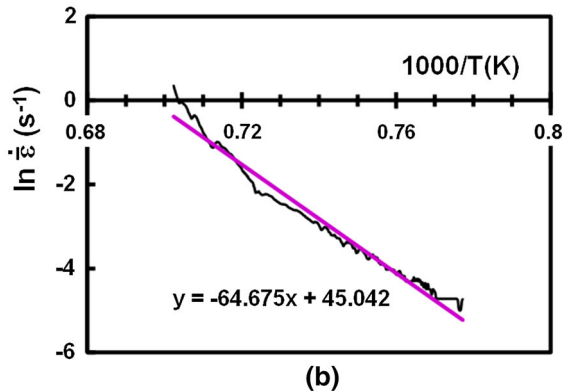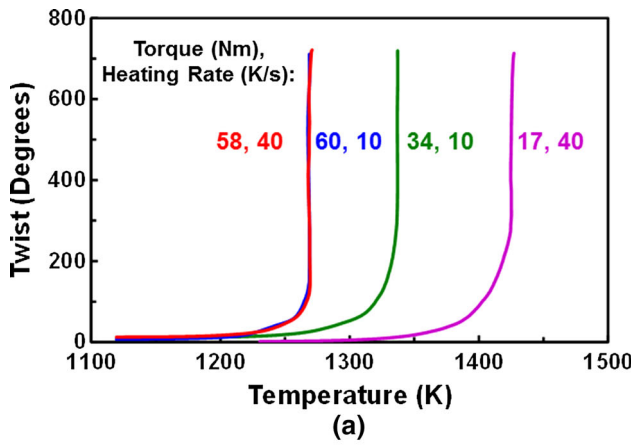
Fig. 12—Experimental data from constant-torque, continuous-heating torsion tests: (a) Twist vs temperature for four combinations of torque/heating rate and (b) sample plot of $\ln\dot{\bar{\varepsilon}}$ vs 1000/T for a test performed with a torque of 17 Nm and a heating rate of 40 K/s (40 °C/s).
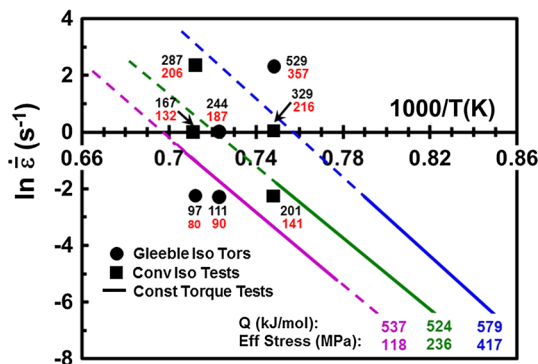

Fig. 13—$\ln\dot{\bar{\varepsilon}}$ vs 1000/T trend lines from constant-torque, continuous-heating Gleeble® torsion tests. The corresponding levels of effective stress and apparent activation energy (Q) for each test are indicated in the figure. Values of peak stress (black numbers) and steady-state flow stress (red numbers) from isothermal tests are also plotted.

which the twist rate began to increase rapidly, on the other hand, was a strong function of torque, however.

Measurements of twist vs temperature were reduced to Arrhenius plots of $\ln\dot{\bar{\varepsilon}}$ vs 1/T (for example, Figure 12(b)). The plots exhibited a small amount of noise, primarily due to the numerical challenge of

determining the instantaneous slope of twist-vs-temperature curves and small variations in torque during each experiment. For $\ln\dot{\bar{\varepsilon}} \leq -2$, the results did indicate an approximately-linear behavior for each of the $\ln\dot{\bar{\varepsilon}}$ vs 1/T graphs (Figures 12(b), 13). (Deviations from linearity for $\ln\dot{\bar{\varepsilon}} > -2$, which corresponded to average imposed effective strains ≥ 0.15, were likely due to the onset of noticeable flow localization; such behavior is currently being quantified experimentally and analytically.) As is common practice, the approximate slopes of the lines in Figures 12(b) and 13 were associated with a specific value of $-Q/R$ from which an apparent activation energy Q was ascertained. For experiments with applied torques of 17, 34, and 60 Nm (corresponding to $\bar{\sigma} = 118$, 236, and 417 MPa, respectively), the apparent activation energies were between 524 and 579 kJ/mol, or values comparable to that derived from the baseline isothermal compression/torsion tests and the nominally-isothermal Gleeble® torsion tests at $\dot{\bar{\varepsilon}} = 1\,\mathrm{s}^{-1}$, i.e., 591 kJ/mol.

By way of comparison, selected values of the peak flow stress (numbers in black) and steady-state flow stress (numbers in red) from the isothermal compression and torsion tests were cross-plotted in Figure 13. Because the linear portions of the $\ln\dot{\bar{\varepsilon}}$ vs 1/T plots corresponded to strains of the order of 0.1, it is not surprising that the peak flow stresses from the isothermal tests showed better agreement with the constant-torque, continuous-heating Gleeble® experiments.

A more quantitative comparison of the isothermal constitutive model and the results from the constant-torque, continuous-heating Gleeble® tests was obtained by recasting Eq. [8] in terms of $\ln\dot{\bar{\varepsilon}}$ vs 1000/T. Taking the natural logarithm of both sides of this expression and re-arranging led to the following relation:

$$\ln\dot{\bar{\varepsilon}} = (-Q/1000R)(1000/T) + n\ln\bar{\sigma} - \ln A - \ln h \quad [11]$$

Inserting the values for Q/R, n, and A from Section III-B-2, Eq. [11] became the following:

$$\ln\dot{\bar{\varepsilon}} = -71.14(1000/T) + 4\ln\bar{\sigma} + 29.73 - \ln h. \quad [12]$$

Neglecting the flow-softening term (ln h), Eq. [12] for effective stresses of 118, 236, and 417 MPa was cross plotted with the trend lines from Figure 13 (Figure 14). For the two higher stress levels, the lines from the two types of tests were almost coincident. This similarity implied that the plastic-flow under constant-torque, continuous-heating conditions mimicked the isothermal, peak-stress behavior as deduced above. On the other hand, the peak stress line from the isothermal tests for the lowest stress level (118 MPa) lay *below* the corresponding line for the constant-torque, continuous-heating experiment (Figure 14). This difference can be rationalized, at least partially, by including the flow-softening contribution, ln h, in Eq. [12]. Per the definition of h in Eq. [9] and assuming
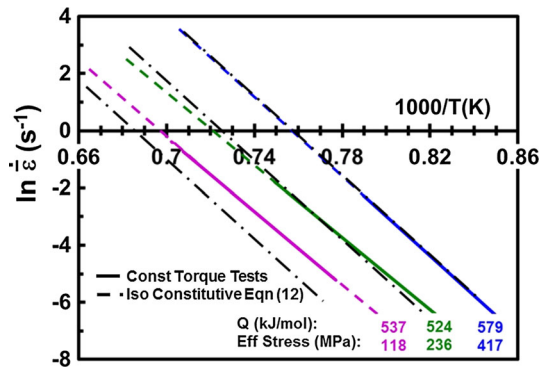
Fig. 14—Comparison of $\ln\dot{\bar{\varepsilon}}$-*vs*-1000/T trend lines from constant-torque, continuous-heating and isothermal Gleeble® torsion tests.
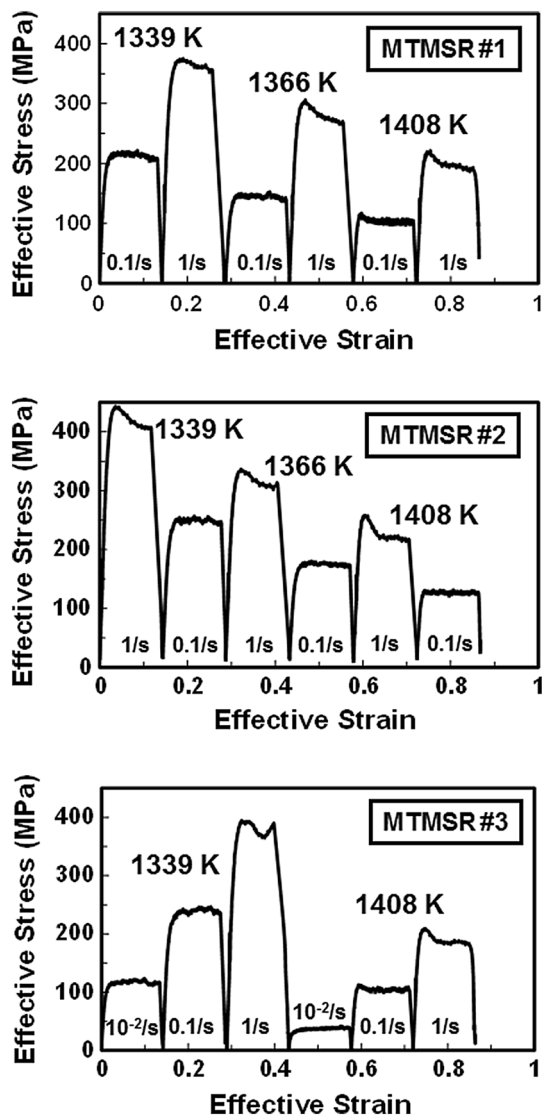

Fig. 15—Effective stress-effective strain curves for LSHR from multi-temperature, multi-strain-rate (MTMSR) Gleeble® torsion tests.

$\bar{\varepsilon}/\bar{\varepsilon}_p = 1/0.05 = 20$ and q = −0.10, −ln h ~ 0.3. Thus, the isothermal-constitutive-equation line in Figure 14 for $\bar{\sigma} = 118$ MPa should be *raised* by a factor of $\ln\dot{\bar{\varepsilon}} = 0.3$. This translation would place that line closer to the constant-torque, continuous-heating trend line for $\bar{\sigma} = 118$ MPa, but still slightly below it.

The Gleeble® torsion samples used in the present constant-torque, continuous-heating experiments were heated to temperatures above the γ' solvus, thus eliminating evidence of microstructure evolution below the solvus. Future research will focus on tests interrupted at various temperatures below the solvus to quantify microstructure evolution and the relative occurrence of dynamic recrystallization.

E. *Multi-Temperature, Multi-Strain Rate (MTMSR) Gleeble® Torsion Tests*

Plots of effective stress *vs* effective strain for Gleeble® torsion testing of individual samples, each at a series of temperatures and strain rates revealed the expected overall trend of decreasing flow stress with a decrease in strain rate and/or an increase in temperature (Figure 15). Furthermore, the levels of flow softening were small to negligible except for strain increments imposed at the highest strain rate used in this type of test, *i.e.*, of 1 s^{-1}. As discussed above, the sources of the softening at this strain rate were deformation heating and DRX.

Because a soak time of 5 or 10 minutes was imposed before each increment of strain ($\approx$0.15), temperature rises generated during prior increments of deformation were dissipated. Thus, a comparison of the data from the MTMSR tests with the *peak* stresses from isothermal tests performed to large strains provided insight into the possible effect of prior strain rate and temperature history on flow behavior. The results for $\bar{\varepsilon} = 0.05$ for the isothermal tests and for an equal strain for each step in the MTMSR tests are summarized in Table VI. The MTMSR entries in the table also indicate whether the imposed strain rate at a given temperature was increased or decreased.

From a broad perspective, the values of the flow stress for 0.1 and 1 s^{-1} from the isothermal and MTMSR experiments were comparable for a given temperature and strain rate (Table VI), thus suggesting the usefulness of the MTMSR approach for high-throughput evaluations. More specifically, for deformation at 1339 K (1066 °C)/0.1 s^{-1}, all of the flow stresses were approximately 220 ± 20 MPa with the Gleeble® torsion data higher (by 11 to 48 MPa) than the isothermal compression/thin-wall torsion results. This trend is the same as that noted in Section III-B-1. MTMSR sample #2 exhibited the highest flow stress under these test conditions (249 MPa) perhaps because it had experienced a prior strain increment at 1 s^{-1} and thus had retained some of its associated harder substructure. Similar trends were noted in the comparison of (softer) isothermal compression/thin-wall torsion and (harder) Gleeble® torsion results at 1339 K (1066 °C), 1 s^{-1}. Among the latter data set, the slightly lower stresses for

Table VI. Flow Stress (MPa) Comparisons at an Effective Strain of 0.05

Test Type	1339 K (1066 °C), 0.1 s^{-1}	1339 K (1066 °C), 1 s^{-1}	1408 K (1135 °C), 0.1 s^{-1}	1408 K (1135 °C), 1 s^{-1}
Iso comp/thin-wall tors	201	329	98	167
Iso Gleeble®, solid-bar tors	237	400	97	169
MTMSR #1 (increasing $\dot{\bar{\varepsilon}}$)	212	366	100	194
MTMSR #2 (decreasing $\dot{\bar{\varepsilon}}$)	249	409	122	216
MTMSR #3 (increasing $\dot{\bar{\varepsilon}}$)	238	375	102	184

MTMSR #1 and MTMSR #3 (relative to the other Gleeble® torsion tests) might be ascribed to some degree of experimental scatter as well as the fact that such deformations had been preceded by straining at a lower rate and thus could have retained a softer substructure during the reloading. Further evaluations are warranted to verify such a hypothesis.

The isothermal compression/thin-wall torsion results at 1408 K (1135°C)/ 0.1 and 1 s^{-1} were very similar to those from the isothermal Gleeble® torsion tests except in a few cases (Table VI). For the 0.1 s^{-1} data, only test MTMSR #2 had a higher flow stress, again a result perhaps of deformation at a higher strain rate which had preceded it. The results for 1408 K (1145 °C)/1 s^{-1} showed reasonable agreement except for the value from MTMSR #2, which may be a result of material variability within the large-diameter extrusion.

IV. CONCLUSIONS

The high-temperature plastic-flow behavior of the powder-metallurgy superalloy LSHR under nominally-isothermal and transient-heating conditions was determined using a variety of test techniques. The following conclusions were drawn from this work:

1. The flow behaviors determined from isothermal hot-compression and thin-wall-torsion tests are essentially identical in terms of von Mises effective stress and strain.
2. The nominally-isothermal torsion testing of solid bars in a direct-resistance-heating Gleeble® machine yields flow curves which are comparable to or slightly higher than those from isothermal compression and thin-wall torsion tests despite the assumption of a uniform *radial* temperature in the Fields-and-Backofen equation employed to reduce torque-twist data to shear stress-shear strain and effective stress-effective strain.
3. A flow-localization analysis can be used to establish the effect of an initial axial temperature gradient on non-uniform plastic flow during nominally-isothermal Gleeble® torsion tests. The analysis reveals that the effective stress-strain curve derived from measurements of torque and twist in a Gleeble® torsion test is almost identical to that for a test with a uniform initial temperature equal to the average temperature in the sample preheated non-uniformly. Flow-localization analysis can also be used to establish the relative contributions of deformation heating and dynamic microstructural changes (*e.g.*, dynamic recrystallization) on flow-softening behaviors observed in Gleeble® torsion tests with an initial axial temperature gradient.
4. Relative to the behavior observed in isothermal tests, the flow stress of LSHR determined from "on-heating" Gleeble® torsion tests can be measurably higher due the retention of a non-equilibrium volume fraction of γ', a finer γ grain size, and perhaps residual substructure from lower-temperature pre-processing. The significant effect of non-equilibrium microstructure on flow stress can be especially crucial for the FEM simulation of solid-state joining process with heating rates of the order of 100 K/s (100 °C/s).
5. A novel torsion test based on the application of a constant torque under continuous (constant-rate) heating conditions can be used to establish constitutive parameters (*e.g.*, apparent activation energy) using a single or limited number of samples. For LSHR, the constitutive parameters from such tests mirror those from more extensive isothermal torsion and compression tests. Data from this type of test can be especially useful for modeling plastic flow during metalworking operations involving concurrent heating and deformation such as a variety of solid-state joining operations.
6. Multi-temperature, multi-strain-rate (MTMSR) Gleeble® torsion tests provide another attractive method for obtaining flow-stress data for constitutive modeling using a limited number of test samples, at least for powder-metallurgy superalloys such as LSHR.

REFERENCES

1. S. Kobayashi, S.-I. Oh, and T. Altan: *Metal Forming and the Finite Element Method*, Oxford University Press, New York, 1989.
2. T. Altan, S.-I. Oh, and H.L. Gegel: *Metal Forming: Fundamentals and Applications*, ASM International, Materials Park, 1983.
3. T. Altan, G. Ngaile, and G. Shen: *Cold and Hot Forging: Fundamentals and Applications*, ASM International, Materials Park, 2004.
4. D.U. Furrer and S.L. Semiatin, eds.: *ASM Handbook Volume 22A: Fundamentals of Modeling for Metals Processing*, 10th ed., ASM International, Materials Park, 2009.
5. D.U. Furrer and S.L. Semiatin, eds.: *ASM Handbook Volume 22B: Metals Process Simulation*, 10th ed., ASM International, Materials Park, 2010.
6. G.E. Dieter, H.A. Kuhn, and S.L. Semiatin, eds.: *Handbook of Workability and Process Design*, ASM International, Materials Park, 2003.
7. G. Shen, S.L. Semiatin, E. Kropp, and T. Altan: *J. Mater. Process. Technol.*, 1992, vol. 33, pp. 125–39.
8. S.L. Semiatin, F. Montheillet, G. Shen, and J.J. Jonas: *Metall. Mater. Trans. A*, 2002, vol. 33A, pp. 2719–27.
9. D.D. Kautz: *ASM Handbook Volume 6A: Welding Fundamentals and Processes*, ASM International, Materials Park, 2011, pp. 179–85.
10. M.B. Uday, M.N. Ahmad Fauzi, H. Zuhailawati, and A.B. Ismail: *Sci. Technol. Weld. Join.*, 2010, vol. 15, pp. 534–58.
11. P.D. Nicolaou, R.E. Bailey, and S.L. Semiatin: in *Handbook of Workability and Process Design*, G.E. Dieter, H.A. Kuhn, and S.L. Semiatin, eds., ASM International, Materials Park, 2003, pp. 68–85.
12. H.G. Suzuki and H. Fujii: *ISIJ Int.*, 1991, vol. 31, pp. 814–19.
13. H.G. Suzuki and D. Eylon: *ISIJ Int.*, 1993, vol. 33, pp. 1270–74.
14. H.G. Suzuki and D. Eylon: *Mater. Sci. Eng. A*, 1998, vol. 243A, pp. 126–33.
15. F.F. Noecker, II and J.N. DuPont: *Weld. J.*, 2009, vol. 88 (#1), pp. 7s–20s.
16. S. Shi, J.C. Lippold, and J. Ramirez: *Welding Journal*, 2010, vol. 89 (#10), pp. 210s–17s.
17. S.S. Babu, J. Livingston, and J.C. Lippold: *Metall. Mater. Trans. A*, 2013, vol. 44A, pp. 3577–91.
18. O.N. Senkov, D.W. Mahaffey, S.L. Semiatin, and C. Woodward: *Metall. Mater. Trans. A*, 2014, vol. 45A, pp. 5545–61.
19. O.N. Senkov, D.W. Mahaffey, S.L. Semiatin, and C. Woodward: *J. Mater. Eng. Perform.*, 2015, vol. 24, pp. 1173–84.
20. D.W. Mahaffey, O.N. Senkov, R. Shivpuri, and S.L. Semiatin: *Metall. Mater. Trans. A*, 2016, vol. 47A, pp. 3981–4000.
21. J. Gayda, T.P. Gabb, and P.T. Kantzos: in *Superalloys 2004*, K.A. Green, T.M. Pollock, H. Harada, T.E. Howson, R.C. Reed, J.J. Schirra, and S. Walston, eds., TMS, Warrendale, 2004, pp. 323–30.
22. J. Lemsky: Report NASA/CR-2005-213574, Ladish Company, Inc., Cudahy, WI, February 2005. http://gltrs.grc.nasa.gov).
23. S.L. Semiatin, K.E. McClary, A.D. Rollett, C.G. Roberts, E.J. Payton, F. Zhang, and T.P. Gabb: *Metall. Mater. Trans. A*, 2012, vol. 43A, pp. 1649–61.
24. S.L. Semiatin, K.E. McClary, A.D. Rollett, C.G. Roberts, E.J. Payton, F. Zhang, and T.P. Gabb: *Metall. Mater. Trans. A*, 2013, vol. 44A, pp. 2778–98.
25. S.L. Semiatin, J.M. Shank, A.R. Shiveley, W.M. Saurber, E.F. Gaussa, and A.L. Pilchak: *Metall. Mater. Trans. A*, 2014, vol. 45A, pp. 6231–51.
26. S.L. Semiatin, S.-L. Kim, F. Zhang, and J.S. Tiley: *Metall. and Mater. Trans. A*, 2015, vol. 46A, pp. 1715–30.
27. S.I. Oh, S.L. Semiatin, and J.J. Jonas: *Metall. Trans. A*, 1992, vol. 23A, pp. 963–75.
28. U.S. Lindholm, A. Nagy, G.R. Johnson, and J.M. Hoegfeldt: *J. Eng. Mat. Technnol. Trans. ASME*, 1980, vol. 102, pp. 376–81.
29. S.L. Semiatin and J.H. Holbrook: *Metall. Mater. Trans. A*, 1983, vol. 14A, pp. 1681–95.
30. S.C. Shrivastava, J.J. Jonas, and G. Canova: *J. Mech. Phys. Solids*, 1982, vol. 30, pp. 75–90.
31. D.S. Fields and W.A. Backofen: *Proc. ASTM*, 1957, vol. 57, pp. 1259–72.
32. S.L. Semiatin and J.J. Jonas: *Formability and Workability of Metals: Plastic Instability and Flow Localization*, ASM International, Materials Park, OH, 1984.
33. S.L. Semiatin, N. Frey, N.D. Walker, and J.J. Jonas: *Acta Metall.*, 1986, vol. 34, pp. 167–76.
34. F. Montheillet and J.J. Jonas: *Metall. Mater. Trans. A*, 1996, vol. 27A, pp. 3346–48.
35. Y. Ning, Z. Yao, X. Liang, and Y. Liu: *Mater. Sci. Eng. A*, 2012, vol. A551, pp. 7–12.
36. M. Detrois, R.C. Helmink, and S. Tin: *Mater. Sci. Eng. A*, 2013, vol. A586, pp. 236–44.
37. L. Briottet, J.J. Jonas, and F. Montheillet: *Acta Mater.*, 1996, vol. 44, pp. 1665–72.